# Interplay between membrane imperfections and external concentration polarization

Arnout D'Haese[1,2] and Andriy Yaroshchuk[3,4]

[1]Particle and Interfacial Technology group (PaInT), Department of Green Chemistry & Technology, Faculty of Bioscience Engineering, Ghent University, Coupure Links 653, B-9000, Ghent, Belgium
[2]CAPTURE, Frieda Saeysstraat 1, 9052 Gent, Belgium, www.capture-resources.be
[3]Dept. of Chemical Engineering, Polytechnic University of Catalonia – Barcelona Tech, av. Diagonal 647, 08028 Barcelona, Spain
[4]ICREA, pg. L.Companys 23, 08010 Barcelona, Spain

**Abstract**

Reverse osmosis membranes provide a highly effective and efficient barrier against various kinds of pollutants. Their reliability depends on the integrity of the active layer: in case the active layer is damaged and contains imperfections, unfiltered feed solution can contaminate the permeate. Various types of integrity monitoring techniques have been developed to verify membrane performance, of which the rejection of fluorescent dyes is a well-established technique. Fluorescent dyes are however relatively small solutes for which the membranes can display non-zero diffusive permeability, such that not all dye passage can be attributed to membrane imperfections. Additionally, fluorescent dyes are subject to external concentration polarization (ECP) during filtration, causing a flux-dependent enrichment at the membrane surface, further complicating the analysis of dye rejection data. This study presents a model to discern between membrane permeability, enrichment by ECP and passage through imperfections. The consequences of imperfections on solute passage are explored, showing that imperfections only contribute significantly to the passage of solutes with a low membrane permeability. This leads to underestimates of the external mass transfer coefficient, with the error being increasingly large with decreasing membrane permeability coefficient, relative to the case of an imperfection-free membrane. This error is then related to the proportionality of the Sherwood number, used to calculate external mass transfer coefficients, with solute diffusivity, allowing the quantification of the contribution of imperfections to water flux. The model was experimentally verified using Pyranine rejection in two membrane types, both operated in a lab-scale flat sheet crossflow test system, finding proof of imperfections in one membrane type.

**Keywords**— reverse osmosis, imperfections, external concentration polarization

# 1 Introduction

In water sanitation, membranes provide an efficient physical barrier against pathogens and pollutants, be it for wastewater treatment, drinking water or process water production. Of the different types of membranes, reverse osmosis membranes are the most selective and can be expected to provide an absolute barrier against pathogens and reduce the concentration of organic micropollutants by 2 orders of magnitude. Their active layer is non-porous, i.e. transport occurs through random voids between polymer segments which are below 0.5 nm in size, while the smallest viral particles are about 2 orders of magnitude larger. In practice, the removal of micro-organisms and other large contaminants is expressed as log removal value (LRV), defined as:

$$LRV = log_{10}\left(\frac{c_f}{c_p}\right) \tag{1}$$

The measurable LRV is usually limited to 6-7 for viral particles, set by the limit of quantification of micro-organisms in the permeate [1, 2, 3], i.e. intact RO membranes produce permeate with concentrations of viral particles below the quantification limit. For dissolved solutes, the LRV is usually in the range of 2-4 [1, 4, 5, 6], since RO membranes display a non-zero permeability towards dissolved solutes. Because of their high selectivity, RO membranes are indispenseable in wastewater reuse schemes.

If the active layer is breached or chemically degraded, larger pores are formed through which pollutants (and potentially pathogens) can permeate. To detect such imperfections, a range of integrity monitoring techniques have been developed. These include direct integrity monitoring, where pressure or vacuum decay over time is measured [7]. The class of so-called indirect integrity monitoring consists of measuring the passage of indicator substances which are expected to be well-rejected by intact membranes. Such indicators include microbial surrogates, such as non-pathogenic viruses and nanoparticles, and smaller molecules such as fluorescent dyes, naturally present organic matter or sulfate ions. Indicators can be spiked into the feed, e.g. the widely used MS2 bacteriophage or fluorescent dyes [4, 2, 8, 6, 5], or can be naturally present, such as qPCR-based detection of naturally present viruses in surface water [3] or fluorometry of fluorescent natural organic matter (NOM) [9]. Spiking can be continuous or pulsed [10], with pulsed spiking enabling both higher sensitivity due to the high feed concentration at its peak, and overall savings in the amount of tracer to be dosed to the feed solution. We will focus here on fluorescent dyes as integrity indicators, since they are inexpensive, can be analyzed easily and in real-time, and they are conservative indicators (i.e. early indicators for membrane damage) [6, 8].

Since membranes display a non-zero permeability towards dissolved solutes, including relatively small organic molecules such as fluorescent dyes, the passage of such markers cannot be attributed to imperfections only. Thus, methods are needed to distinguish between expected and elevated dye permeation, however, the membrane permeability towards a specific dye is unknown a priori. During solute transport in dense membranes, convective coupling between water and solute fluxes is generally assumed to be negligible, due to the overwhelming friction caused by the active layer polymer [11, 12]. Solute transport through the active layer is therefore commonly modelled as diffusion, according to the

solution-diffusion model, with the solute flux being proportional to the solute concentration difference across the membrane as the sole driving force [11]. This would result in a constant solute flux regardless of water flux. The proportionality between a solute flux and its driving force is given by the membrane permeability coefficient ($B$). $B$ is strongly dependent on solute size: for instance, experimental data of Drazevic et al. [13] suggests that for a series of alcohols in a sea water RO membrane, solute diffusivity within the active layer is proportional to the bulk aqueous diffusivity to the power 11.6. Similar sensitivity has also been found for pervaporation membranes [14] and crosslinked PVA membranes [15]. In turn, $B$ is proportional to solute diffusivity within the active layer [16]. Thus, a modest increase in solute size (decrease in bulk aqueous diffusivity) results in a strong decrease of solute diffusivity within the active layer.

Based on the preceeding description of a membrane's active layer, one would expect a rather sharp cut-off of molecular weight or size above which solute permeability quickly becomes negligibly small. In practice however, noticeable passage of relatively large solutes is often seen during filtration, as is evidenced by the relatively modest LRV values commonly found for fluorescent dyes [4, 5] or detection of NOM molecules in RO permeate of a full-scale installation with an estimated molecular weight of 5000 Da [9]. We identify here two possible causes for this phenomenon, and how these causes interact. The first possibility is external concentration polarization (ECP). ECP causes the accumulation of rejected solutes at the membrane-feed solution interface. ECP is a steady-state process, in which the accumulation is balanced by back diffusion of solutes towards the bulk feed. Back diffusion in turn is aided by high crossflow velocity and turbulence in the feed flow channel. The external hydraulic conditions and solute diffusivity are combined in a single variable, $k$, the external mass transfer coefficient, which can be calculated using an appropriate Sherwood relation [17]:

$$k = \frac{Sh \cdot D}{d_h} = \frac{D}{d_h} \cdot a \cdot Re^b \cdot Sc^c \cdot \left(\frac{d_h}{L}\right)^d \tag{2}$$

Depending on the hydraulic conditions, different empirical values for $a...d$ can be chosen [17, 18, 19], and $k$ can also be determined experimentally [20]. Since back diffusion relies on the solute's diffusivity, ECP will be worse for larger solutes. Worse ECP implies a higher solute concentration at the membrane surface and thus a higher transmembrane solute flux as well, if the solute's permeability is non-zero. This introduces an exponential proportionality between solute flux and water flux. For a given solute, the membrane permeability coefficient and ECP modulus both correlate with solute size, but oppositely so. Consequently, ECP dulls the membrane's cut-off, with an exponential proportionality to water flux. Although the magnitude of ECP can be controlled by the design of the feed flow channel and operating conditions, it cannot be avoided entirely.

The second possible cause for the passage of large solutes is the presence of imperfections in the membrane's active layer, as is demonstrated by incrementally damaging membranes [21, 10, 22]. In this study, we define imperfections as spots in the active layer where the active layer polymer is absent or significantly degraded, such that imperfections are not selective anymore towards solutes small enough to pass through them. We will further only consider relatively small imperfections here, with a diameter much smaller than the thickness

of the ECP boundary layer, such that the imperfections do not interrupt this boundary layer. Such imperfections would be in the range of ten to a few tens of nanometer in diameter.· The implications and shortcomings of this assumption will be discussed in more detail in Section 4.2. Solute transport through imperfections thus occurs through convective coupling with the water flux through those imperfections. Consequently, the solute flux through imperfections will increase proportionally with the water flux. This is in contrast to diffusive solute transport through the intact active layer, where a solute flux independent of the water flux is expected. However, ECP is causing an exponential accumulation of solutes at the membrane surface as a function of water flux, such that the solute flux will also show a dependence on water flux, even in the case of purely diffusive transport. This renders it difficult to differentiate between diffusive and convective solute transport. Additionally, the increased solute concentration at the membrane surface caused by intact active layer will increase the solute flux through nearby imperfections, increasing the proportionality of solute flux to water flux. The ECP modulus can be calculated using an appropriate Sherwood relation, which in turn can be calibrated using experiments. These experiments however, are commonly performed using small solutes such as NaCl [17, 20], whose diffusivity is up to 10 times higher than that of larger fluorescent dyes. Differences in solute diffusivity are accounted for by the Schmidt number and its exponent, however, as will be shown below, the presence of small imperfections causes mass transfer coefficient estimates to deviate, specifically for larger solutes. This presents us with a chicken-or-egg problem: if present, imperfections influence estimates of the external mass transfer coefficient of larger solutes, while the correct external mass transfer coefficient is needed to differentiate between ECP and imperfections.

The aim of this study is to untangle the contributions of ECP, imperfections and membrane permeability to the transport of fluorescent dyes, commonly used for membrane integrity monitoring. We present a transport model that accounts for imperfections and external concentration polarization simultaneously. The consequences of imperfections for solute passage and external mass transfer estimates are explored, where it is shown that the influence is large for solutes having a low membrane permeability, and vice versa. We propose a method to quantify imperfections, based on external mass transfer coefficient estimates of at least 2 solutes: one of high and one of low membrane permeability. Crucially, neither the external mass transfer coefficient nor the membrane permeability of the solutes needs to be known a priori. The sensitivity of the estimate of imperfections is tested with respect to error propagation in experimental data and intact membrane permeability, showing that low membrane permeability is necessary for reliable estimates of imperfections. The model is experimentally tested using 2 RO membrane types, a high selectivity and a high permeability type, finding experimental evidence of imperfections in the high permeability membrane.

# 2 Theory

In the following analysis, imperfections are not defined in size and number but are included as a fractional contribution to volume flow, denoted $f_i$:

$$f_i = \frac{J_{vi}}{J_v + J_{vi}} \tag{3}$$

As such, the analysis remains broadly applicable. We assume here that imperfections are small, much smaller than the thickness of the ECP boundary layer, and evenly distributed along the membrane surface. We further assume that the imperfections are scarce, such that the distance between them is large and they do not influence each other. This implies that the solute concentration in the ECP boundary layer is constant parallel to the membrane, i.e. there are no concentration gradients in the boundary layer in the plane of the membrane. The implications of these assumptions will be discussed in more detail in section 4.2. The imperfections considered in this study would roughly fall in the range of 5 to 500 nm in diameter. Smaller pores could display some selectivity against dissolved solutes, while larger imperfections would distort the local ECP modulus too much for the analysis presented below to hold.
Fluxes in an imperfection-bearing membrane are compound fluxes, composed of fluxes through the intact active layer and fluxes through imperfections. Fluxes through the intact active layer are modelled according to the solution-diffusion model, so that in the intact active layer, there is no frictional coupling between solvent and solute fluxes. In imperfections, water and solute fluxes are assumed to be fully coupled. Although in principle, there is also a diffusive component to the solute flux through an imperfection [23], it can be shown that the diffusive contribution quickly tends to zero for pores of a diameter above 5 nm at pressures relevant for reverse osmosis [24]. The solute flux including imperfections is then given by:

$$\langle J_s \rangle = J_v c_p + J_{vi} c_m \approx J_v (c_p + f_i c_m) \tag{4}$$

where $J_{vi}$ was substituted using Eq. 3, and $1 - f_i \approx 1$ since $f_i << 1$ for selective membranes. In Eq. 4, $c_m$ is the solute concentration in the ECP boundary layer, implying that imperfections are not selective towards the solutes under consideration.

## 2.1 Film theory applied to a membrane bearing imperfections

External concentration polarization (ECP) is modelled according to film theory [18], in which a steady-state is assumed of convective solute transport towards the membrane surface and backdiffusion of rejected solutes towards the bulk feed solution. The fluxes are supplemented with an additional convective transmembrane solute flux due to imperfections. A scheme of the fluxes in the boundary layer is provided in Fig. 1. Note that the transmembrane solute flux now contains a contribution of imperfections, in the form of $J_v f_i c_m$. The ECP flux balance is then:

$$\langle J_s \rangle = J_v (c_p + f_i c_m) = -D \frac{dc}{dx} + J_v c(x) \tag{5}$$

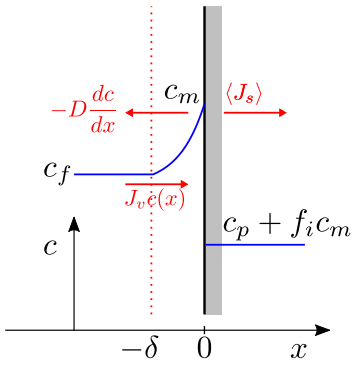


Figure 1: Scheme of fluxes in the external concentration polarization boundary layer, including a convective transmembrane flux caused by imperfections ($f_i c_m$).

The integration limits are:

$$\begin{cases} x = -\delta \Leftrightarrow c = c_f \\ x = 0 \Leftrightarrow c = c_m \end{cases}$$

$c_p$ in Eq. 5 does not include the increase in solute concentration in the bulk permeate originating from imperfections, while imperfections do lower the average interface concentration on the feed side, $c_m$. The solute flux through intact active layer is driven by the concentration gradient across it, from which it follows that an increase of $c_p$ at the permeate-side interface would suppress $J_s$. This could happen if solutes permeating through imperfections are transported laterally within the support layer in a hemispherical flow pattern. We expect transport within the support layer in the lateral direction to be strongly hindered, and the local lateral water velocity to decrease by $1/r^2$ with $r$ being the radius of the hemisphere. In addition, the water flux, in the normal direction, distorts the hemispherical flow pattern, so that solutes can only reach the support-side of the active layer by diffusing against the direction of volume flux. This gives rise to internal concentration polarization (ICP), which is particularly severe in RO membranes due to their relatively thick support layers [25] and high water fluxes. Additionally, in the context of integrity monitoring, large solutes are commonly used having a low diffusivity, further excarebating ICP. Therefore, we consider $c_p$ at intact active layer independent from solutes permeating through imperfections.
Integrating Eq. 5 results in:

$$\exp\left(\frac{J_v}{k}\right) = \frac{c_m(1-f_i) - c_p}{c_f - f_i c_m - c_p} \tag{6}$$

In Eq. 6, $c_p$ is substituted according to the solution-diffusion model [11]:

$$c_p = c_m \frac{B}{J_v + B} \tag{7}$$

This substitution allows us to calculate the surface concentration $c_m$ as a function of flux, external mass transfer coefficient $k$, membrane permeability $B$ and $f_i$:

$$c_m = c_f \frac{(J_v + B)\exp\left(\frac{J_v}{k}\right)}{J_v + B\exp\left(\frac{J_v}{k}\right) + f_i(J_v + B)\left(\exp\left(\frac{J_v}{k}\right) - 1\right)} \tag{8}$$

## 2.2 Solute flux and observable rejection with imperfections

The overall solute flux, given by Eq. 4, can be calculated by substitution of $c_p$ and $c_m$ by Eqs. 7 and 8 respectively:

$$\langle J_s \rangle = c_m(J_v + J_{vi})\left((1 - f_i)\frac{B}{J_v + B} + f_i\right) \approx c_m\left(\frac{B}{J_v + B} + f_i\right) \tag{9}$$

where we again used the approximation of $1 - f_i \approx 1$. Observable rejection ($R_o$) is defined as the rejection calculated using bulk solution concentrations, in contrast to the real rejection, which is determined by interface concentrations but is experimentally inaccessible. The observable rejection is given by:

$$R_o = 1 - \frac{c_p}{c_f} = \frac{J_v - f_i(J_v + B)}{J_v + B\exp\left(\frac{J_v}{k}\right) + f_i(J_v + B)\left(\exp\left(\frac{J_v}{k}\right) - 1\right)} \tag{10}$$

and observable passage ($S_o$) by:

$$S_o = \frac{c_p}{c_f} = \frac{(B + f_i(J_v + B))\exp\left(\frac{J_v}{k}\right)}{J_v + B\exp\left(\frac{J_v}{k}\right) + f_i(J_v + B)\left(\exp\left(\frac{J_v}{k}\right) - 1\right)} \tag{11}$$

In Eqs. 10 and 11, the presence of imperfections causes observable rejection to decrease and observable passage to increase, as expected. Note that setting $f_i = 0$ in Eqs. 10 and 11 reduces to them to observable rejection and passage for imperfection-free membranes:

$$R'_o = \frac{J_v}{J_v + B\exp\left(\frac{J_v}{k}\right)} \tag{12}$$

$$S'_o = \frac{B\exp\left(\frac{J_v}{k}\right)}{J_v + B\exp\left(\frac{J_v}{k}\right)} \tag{13}$$

Eqs. 12 and 13, and equations derived from them, will be used as a benchmark with which the performance of imperfection-bearing membranes is compared. The ratio of Eq. 13 by Eq. 12 can be transformed into the following expression [20]:

$$\ln\left(\frac{S'_o J_v}{R'_o}\right) = \ln(B) + \frac{J_v}{k} \tag{14}$$

which yields a straight line as a function of $J_v$, allowing one to estimate $B$ and $k$ simultaneously from the intercept and slope respectively. A similar transformation of Eqs. 10 and 11, including imperfections, results in:

$$\ln\left(\frac{S_o J_v}{R_o}\right) = \ln\left(\frac{J_v(B + f_i(J_v + B))}{J_v - f_i(J_v + B)}\right) + \frac{J_v}{k} \tag{15}$$

Eq. 15 can be simplified: since $B << J_v$, $J_v + B \approx J_v$, and since $f_i << 1$, the numerator becomes: $J_v - f_i(J_v + B) \approx J_v(1 - f_i) \approx J_v$, so that:

$$\ln\left(\frac{S_o J_v}{R_o}\right) \approx \ln(B + f_i J_v) + \frac{J_v}{k} \tag{16}$$

Note that $f_i J_v$ is not necessarily (much) smaller than $B$ since the values of these 3 variables are independent from each other. In the case of a perfect membrane, the plot $\ln(S_o J_v / R_o)$ as a function of flux yields a straight line for a given solute and a given crossflow rate. When imperfections are present, the plot becomes logarithmic instead of linear. This is a clear indication of convective transport through imperfections.

## 2.3 Susceptibility of solute transport to imperfections

The sensitivity of solute transport to imperfections increases with decreasing membrane permeability for a given solute. This can be graphically illustrated using Eqs. 16 and 14 for defect-bearing and defect-free membranes respectively. Eq. 14 yields a straight line as a function of water flux for defect-free membranes, while the corresponding equation for defect-bearing membranes (Eq. 16) is a logarithmic function of water flux. Imperfections are accounted for in the term $\ln(B + f_i J_v)$, while the corresponding term for a perfect membrane is simply $\ln(B)$. It follows that imperfections are only noticeable when $f_i J_v$ approaches $B$, which can occur at high flux, high $f_i$ and/or low $B$. In the case of NaCl, the permeability coefficient of RO membranes is typically in the range of $10^{-8}$ - $10^{-7}$ m/s, which implies that $f_i$ needs to be $10^{-3}$ - $10^{-2}$ before the term $f_i J_v$ becomes significant at practical fluxes. Therefore, conductivity measurements are inherently not sensitive enough to detect imperfections contributing 0.1% or less to the total flux. If however 0.1% of the permeate is in fact unfiltered feed solution, the membrane will most likely show unacceptably high breakthrough of pollutants and small particles, potentially including pathogens.

## 2.4 Influence of imperfections on external mass transfer coefficient estimates

External concentration polarization and imperfections both cause solute flux to vary with water flux. They do so by a different mechanism: ECP causes an exponential increase of solute concentration at the membrane surface, while the convective flux through imperfections is a linear function of water flux. Therefore, imperfections will interfere with experimental estimates of the external mass transfer coefficient, based on observable rejection and water flux.
Observed rejection from an imperfection-bearing membrane will obey Eq. 16, where the external and transmembrane transport is characterized by $k$, and $B$ and $f_i$ respectively. When solute transport through an imperfection-bearing membrane is modelled using Eq. 14, assuming a perfect membrane, one obtains the estimates $B'$ and $k'$. $B'$ and $k'$ are incorrect, and differ from the correct $B$ and $k$ with the following relation existing between them:

$$\ln(B') + \frac{J_v}{k'} = \ln(B + f_i J_v) + \frac{J_v}{k} \tag{17}$$

which can be rearranged into:

$$\ln\left(\frac{B'}{B+f_iJ_v}\right) = \frac{J_v}{k} - \frac{J_v}{k'} \tag{18}$$

What we are interested in is how $B'$ and $k'$ change relative to $B$ and $k$ with increasing $f_i$. Since there are 2 unknowns, we will analyse both variables separately, assuming the other unknown constant. To study $B'$, we assume that $k' = k$. It follows from Eq. 18 that $\frac{B'}{B+f_iJ_v} = 1 \Leftrightarrow B' = B + f_iJ_v$. Thus, $B'$ will be an overestimate of $B$, increasingly so with higher $f_i$, and will show a weak flux dependence. Assuming now that $B' = B$, the left-hand side of Eq. 18 shows: $\frac{B'}{B+f_iJ_v} < 1$ so that the natural logarithm is a negative number. It then follows that $\frac{J_v}{k} < \frac{J_v}{k'} \Leftrightarrow k > k'$. Thus, $k'$ will be an underestimate of the actual mass transfer coefficient. An imperfection-bearing membrane will thus appear as more permeable and more impacted by ECP than expected. This will again only be the case if the term $f_iJ_v$ is significant relative to $B$, as can be seen in the left-hand side of Eq. 18. Thus, external mass transfer coefficient estimates for small solutes having a relatively high membrane permeability will be correct regardless of imperfections, while the external mass transfer coefficient estimates for larger solutes will be underestimated if the membrane bears imperfections.

# 3 Materials and Methods

## 3.1 Experimental protocol

RO filtration experiments were performed using a flat sheet, multichannel cell holding 4 coupons in parallel. Flow channel dimensions are 20 mm wide, 100 mm long and 1.5 mm high. 2 membrane types were tested: ESPA2 BWRO (Hydranautics, USA) and FT30 (Filmtec - Dupont, USA). Membrane coupons were harvested from spiral wound elements. The ESPA2 module was a fiberglass-encased element, delivered dry; the FT30 element was mesh-wrapped and delivered wet. Although opening up spiral wound elements risks damaging the membranes inside, the authors have noticed that flat sheet samples (received as such) tend to perform worse in terms of selectivity than harvested coupons. This could be due to the membranes inside spiral wound elements being shielded from particulates, light and friction. To avoid puncturing the membrane coupons during cell assembly, no feed spacers were used in this experiment. Since the relatively long and thin flow channel does not contain a spacer, laminar flow is expected at a Reynolds number $< 2000$. At 0.05 - 0.4 m/s crossflow velocity used in this study, the Reynolds number was 157 - 1256, within the laminar flow range.

Prior to fluorophore rejection tests, the membranes were compacted at 20 bar during 4 hours. The feed solution consisted of 0.1M NaCl and 1 mg/L pyranine. Samples were collected after at least 30 minutes of equilibration after adjusting feed pressure and/or crossflow velocity; permeate not collected for analysis was returned to the feed solution. NaCl rejection was measured using electrical conductivity. Pyranine rejection was measured using a Tecan M200Pro 96 well plate reader, at 370 nm excitation and 515 emission wavelengths. Both feed and permeate samples were buffered at pH 8 prior to fluorescence analysis, as

pyranine's fluorescence intensity is pH-dependent [26]. Permeate samples were spiked with a concentrated NaCl solution, such that the salinity of feed and permeate samples was (nearly) equal. Method development had shown that NaCl up to 0.1M does not quench pyranine fluorescence.
RO experiments were carried out between 6 and 20 bar for ESPA2 and between 8 and 35 bar for FT30, yielding fluxes between 0.9 and $25{\cdot}10^{-6}$ m/s (3 to 80 lmh), at a crossflow velocity of 0.4 m/s. At the highest pressure, crossflow was varied between 0.05 and 0.4 m/s. The wide range of operating conditions results in a highly variable ECP modulus. Temperature was fixed at 25°C using a heat exchanger coupled to a thermostat recirculator (AP15R, VWR).

### 3.2 Diffusivity measurement of Pyranine

The 2D DOSY experiments were performed using the "dstegp3s" pulse program from the standard Bruker library (double pulsed field gradient stimulated echo sequence). The spectral width used was 20 ppm with 8 or 16 scans (depending on the sample) of 32K data points each being accumulated, preceded by 4 dummy scans. A relaxation delay of 1s and eddy current delay of 5ms were used and the spectrometer excitation frequency ($O_1$) was set to 6.175 ppm. 32 increments were measured varying the gradient strength from 2% to 98% in a linear fashion. Diffusion time and duration of the gradient pulses were optimized for each sample in order to give an optimal signal intensity decay and accurate fitting. Processing consisted of one order of zero filling to 65K real data points, followed by exponential apodisation using a 0.30 Hz line broadening factor prior to Fourier transformation, followed by phase correction and a zero-order base line correction. The diffusion coefficients could then be fitted to the data using the Stejskal-Tanner equation.
All spectra were recorded on an Avance III HD Bruker spectrometer operating at 1H frequency of 500.08MHz and equipped with a 5mm triple channel TXO $^{1}H/^{n}X/^{19}F$ room temperature probe running Topspin 3.6.2. The sample temperature was set at 25°C and controlled within ± 0.1 °C with a Eurotherm 2000 VT controller. A Pyranine sample was prepared by vacuum drying approx. 10 mg Pyranine and dissolving it in 1 mL of $D_2O$ (99.90% D; Eurisotop, France). The resulting diffusivity in $D_2O$ was $3.88{\cdot}10^{-10}$ $m^2/s$; this was converted to aqueous diffusivity by multiplying with 1.232 to yield $4.78{\cdot}10^{-10}$ $m^2/s$. The correction is needed to account for the higher viscosity of $D_2O$ relative to $H_2O$ [27]. The aqueous diffusivity of $4.78{\cdot}10^{-10}$ $m^2/s$ corresponds to a Stokes diameter of 0.51 nm.

## 4 Results and Discussion

### 4.1 Contribution of imperfections to solute flux

Imperfections are expected to contribute significantly to the flux of larger, low-permeability solutes, and negligibly to smaller, high-permeability solutes. This is because the contribution of imperfections to solute passage is captured in the term $B + f_i J_v$, as shown in Eq. 16, where the contribution of imperfections is only significant if $B$ is small enough. It follows that, for a small enough $B$, even a small number of imperfections can be the dominant pathway for

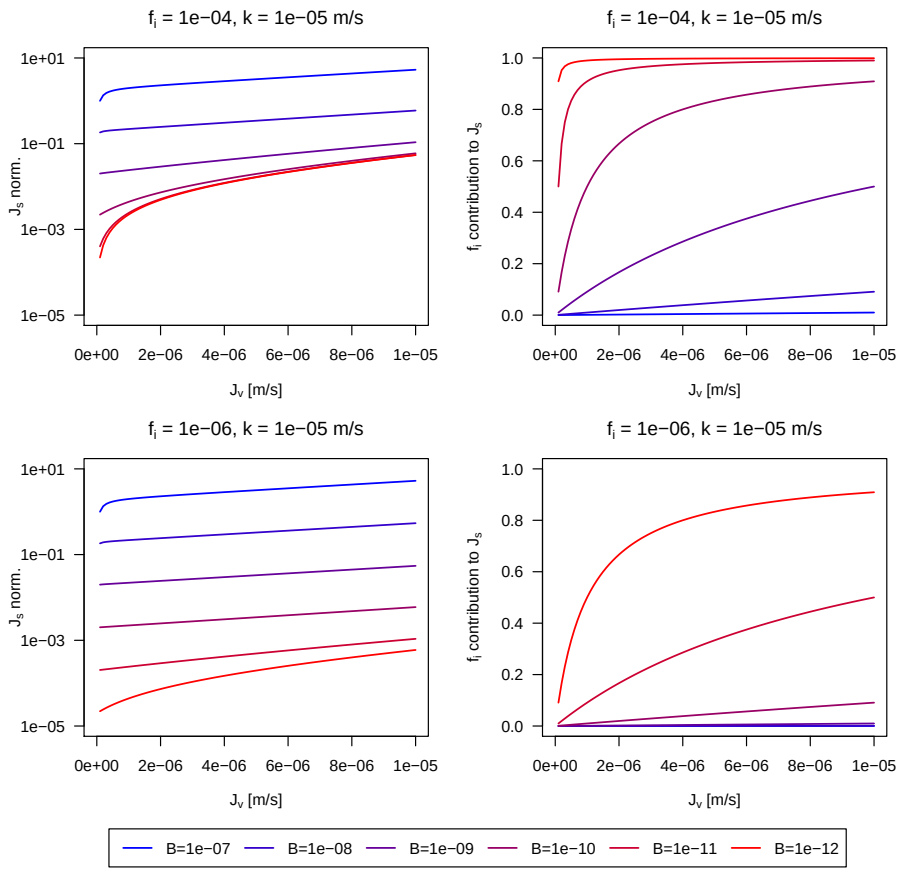


Figure 2: Contribution of imperfections to $J_s$, as a function of $f_i$ (the fractional contribution of imperfections to permeate flux) and membrane permeability coefficient (units: m/s). Left side: solute flux on a log-lin plot, normalized to the most permeable solute, right side: fraction of solute flux originating from imperfections.

solute transport. This range of contributions by imperfections is simulated in Fig. 2, showing the solute flux as a function of water flux for a range of membrane permeability coefficients. The solute fluxes are normalized for the flux of the highest permeability solute. These simulations show that for solutes having a very low membrane permeability, even $f_i$ as low as $1{\cdot}10^{-6}$ contributes in excess of 80% of solute flux at practical water fluxes. Fig. 2 also shows that high permeability solutes are not suited for integrity monitoring: even when imperfections contribute 0.01% to the permeate flow rate, their contribution to solute flux is less than 10% for solutes with a membrane permeability of $1{\cdot}10^{-8}$ m/s. For SWRO membranes, the NaCl permeability coefficient is typically around $5{\cdot}10^{-8}$ m/s, showing that conductivity measurement is not suitable as early-warning of decreased membrane selectivity.

It can also be seen in Fig. 2 that passage of relatively large solutes (small $B$)

becomes independent of their membrane permeability, and thus independent of solute size. Normally there is a very steep proportionality of solute diffusivity within the active layer ($D_m$) with diffusivity in the bulk solution. In turn, the membrane permeability coefficient is linearly proportional to diffusivity within the active layer according to the solution-diffusion model, so the same steep proportionality is expected. For instance, Drazevic et al. [13] measured diffusivity of 6 alcohols in the active layer of SWC4+ SWRO membranes using ATR-FTIR, finding that $D_m$ decreased with almost 2 orders of magnitude with solute size, while the bulk diffusivity decreased by less than 30% for the given set of solutes. This yielded a proportionality of $D_m \propto D^{11.6}$. The exact proportionality will depend on the specific membrane, but for selective membranes, this proportionality should be large in any case. In the case of relatively large solutes permeating through imperfections, this proportionality appears to falls to zero as solute flux is almost entirely through imperfections. The loss of this large proportionality between $D_m$, and thus $B$ with $D$ is a tell-tale sign of imperfections. This was observed by Yoon for a series of integrity monitoring tracers, showing identical passage through a Filmtec BW30 membrane despite differences in molecular weight and size [5]. In Fig. 2, the same external mass transfer coefficient was used for all solutes, for the clarity of presentation. In reality, $k$ and $B$ correlate as well, since they are both functions of solute diffusivity. Thus, larger solutes (having both a lower $k$ and $B$) can display a larger passage than smaller solutes, at practical water fluxes. This is a phenomenon that can only be explained by convective transport through imperfections combined with solute enrichment through ECP.

## 4.2 Effect of model assumptions on solute flux through imperfections

In constructing the model, a few simplifying assumptions were made. The first and most important one is the assumption of a fully homogeneous ECP boundary layer on the feed side, in the plane parallel to the membrane. This assumption therefore relies on vanishingly small Péclet numbers within the ECP boundary layer close to imperfections, i.e. fast lateral diffusion and slow convective transport. In reality, the much higher water flux through an imperfection combined with no slip at the active layer implies that feed solute concentration gradients parallel to the membrane will exist, both at the active layer surface and at some distance away from it. This implies that the feed solution permeating through an imperfection is intermediate in composition between the bulk feed solution and the feed solution at intact membrane surface. It also implies that imperfections located close to each other can influence each other, i.e. when the lateral concentration gradients they produce overlap. The second assumption is that the flux of solute through an imperfection does not influence the normal, solution-diffusion type transport through neighbouring intact active layer. This interaction could occur through lateral convection and diffusion of solutes within the support layer (after membrane passage), decreasing the local transmembrane concentration difference and thus suppressing transport through the active layer. We will focus here on the first assumption only, since we expect that lateral diffusion in the support will be strongly hindered and therefore limited to a small border surrounding an imperfection. Additionally, the membrane permeability coefficient of the solutes under consideration

is small, so the diffusive transmembrane transport is limited in any case.
The extent of homogeneisation in the ECP boundary layer can be explored by studying 2 limiting cases: fully homogeneous (as assumed in Section 2.2) or no diffusion at all between bulk feed solution permeating through an imperfection and the surrounding feed solution within the ECP boundary layer. In the second case, ECP is only considered at the intact active layer while the fluid entering an imperfection is assumed to be bulk feed solution. The second case of fully inhomogeneous boundary layer is typically considered in the solution-diffusion-imperfection model [23]. This second case yields the following expression for observable solute passage:

$$S_o = \frac{B \exp\left(\frac{J_v}{k}\right)(1 + f_i) + f_i J_v}{B \exp\left(\frac{J_v}{k}\right) + J_v} \tag{19}$$

The 2 limiting cases present the lower and upper limit of feed solute transport through imperfections, with the lower limit given by the inhomogeneous boundary layer case. This is shown in Fig. 3, showing observable passage as a function of flux. The transport through imperfections will be in between both limits, with smaller imperfections tending more towards the case of a homogeneous boundary layer and vice versa. More detailed, 2D numerical modelling is underway to quantify the ECP boundary layer in the vicinity of imperfections. The simulations shown in Fig. 3 were performed using $k = 2{\cdot}10^{-5}$ m/s, $B = 1{\cdot}10^{-10}$ m/s and $f_i = 1{\cdot}10^{-5}$. At a practical flux of 10 µm/s (=36 lmh), the upper limit of passage was 25% higher than the lower limit, showing that the uncertainty introduced is limited. With more detailed knowledge, the current model can be supplemented: a higher "effective" external mass transfer coefficient can be assigned to solute transport near an imperfection, which implies less feed solute build-up close to an imperfection.

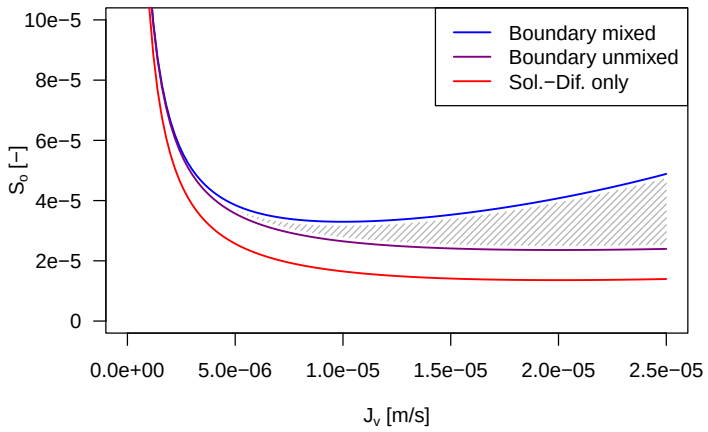


Figure 3: Observed passage through an imperfection-bearing membrane as a function of flux, assuming homogeneous (blue line) or fully inhomogeneous ECP boundary layer (purple line). It is expected that transport through real imperfections will be in between both limiting cases, shown as the gray hatched area. Simulation parameters: $f_i = 1{\cdot}10^{-5}$, $k = 2{\cdot}10^{-5}$ m/s, $B = 1{\cdot}10^{-10}$ m/s.

### 4.3 Errors in external mass transfer coefficient estimates introduced by imperfections

Linearizing solute passage and rejection, as shown in Eq. 14 for imperfection-free membranes, yields estimates for the external mass transfer coefficient $k$ and membrane permeability coefficient $B$. However, as was argued in section 2.4, the presence of imperfections will cause $k$ and $B$ to be underestimated and overestimated, respectively. The magnitude of the error depends on the magnitude of $B$ relative to $f_i J_v$: if $B$ is much larger, imperfections will not have a noticeable impact on estimates, while their impact becomes significant with lower values for $B$. This is illustrated in panel A of Fig. 4, where linearized passage over rejection curves are simulated for 4 solutes, with and without imperfections ($f_i = 10^{-5}$). The true values of $k$ and $B$ were functions of solute diffusivity, with $k \propto D^{0.6}$ and $B \propto D^{10}$. The proportionality of $k$ to $D$ corresponds to an exponent of 0.4 of the Schmidt number in the Sherwood relation (see Eq. 2).

Subsequently, $k$ and $B$ were estimated using linear regression assuming no imperfections, using Eq. 14. The resulting estimates are shown in panel B of Fig. 4, normalized by the true values of $k$ and $B$. As the solute diffusivity decreases (and thus, $B$ decreases), the impact of imperfections becomes significant with $k$ decreasing relative to the true value and $B$ increasing, as predicted in section 2.4. The estimate of $B$ is not impacted nearly as much as the estimate of $k$, especially considering that $B$ is expected to vary by orders of magnitude with modest variations in solute size, in contrast to $k$. The reason for this is that the estimates of $B$ with or without imperfections both converge to the true value of $B$ at zero water flux.

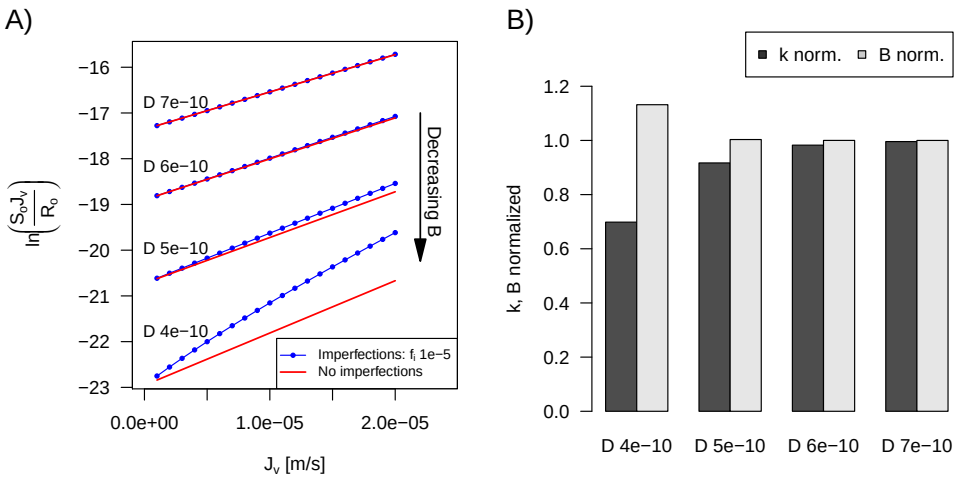


Figure 4: A) Simulated linearized passage over rejection for 4 solutes of increasing size, with and without imperfections in the membrane. The external mass transfer coefficient ($k$) and membrane permeability coefficient ($B$) were calculated from the solutes' diffusivity (see main text). B) $k$ and $B$ of the 4 solutes for the imperfection-bearing membrane, calculated using Eq. 14. The fitted values are normalized by the true $k$ and $B$, showing that imperfections cause $k$ and $B$ to be under- and overestimated respectively, with the error increasing as $B$ decreases.

The large impact of imperfections on the estimates of $k$ for large solutes can also be seen in estimates of the exponent of $D$ in the proportionality of $k \propto D^x$. We can write for $k$ the following function:

$$k = aD^x \quad \Rightarrow \quad \ln(k) = \ln(a) + x\ln(D) \tag{20}$$

allowing $x$ to be calculated by linear regression of $\ln(k)$ as a function of $\ln(D)$. For the above simulations shown in Fig. 4, the estimate of $x$ was 1.23, compared to the true value of 0.6. An exponent of $D$ larger than 1 also implies that the exponent of the Schmidt number in the Sherwood relation would be negative. In contrast, values for the Schmidt number exponent reported in literature are generally in the 0.25 - 0.4 range [28, 17, 29, 30, 19], with 0.33 being the value predicted for fully developed laminar flow according to the Lévêque equation.

## 4.4 Experimental results

The observable passage of NaCl and pyranine as a function of flux is shown in Fig. 5, obtained at a crossflow velocity of 0.4 m/s at varying pressure. Pyranine displayed average LRVs of 2.83 and 3.45, corresponding to a rejection of 99.85 and 99.96 % for ESPA2 and FT30 respectively. Fluorophore rejection in the context of integrity monitoring is preferably around 99.99%, or LRV 4 [21, 4]. NaCl rejection varried between 86.2 - 98.8 and 97.7 - 99.6% for ESPA2 and FT30 respectively. As can be seen in Fig. 5, there is some but limited variability between coupons of the same membrane type.

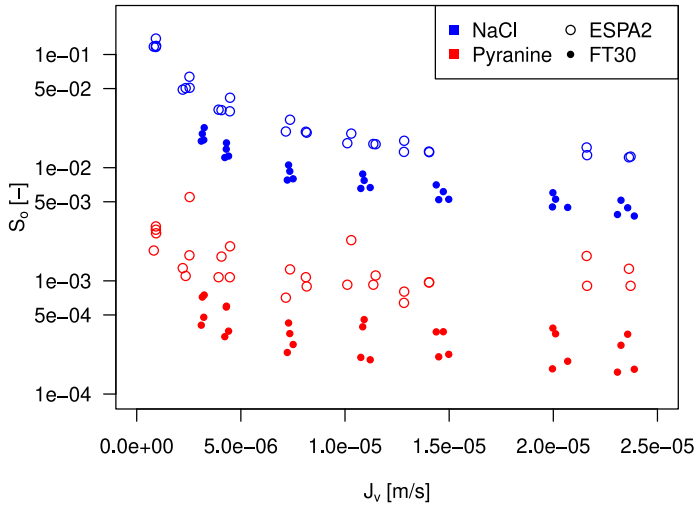


Figure 5: Experimental observable passage of NaCl and pyranine as a function of water flux for both membrane types at 0.4 m/s crossflow velocity. Note the logarithmic Y-axis.

Solute passage for both solutes and both membranes was linearized according to Eq. 14, assuming no imperfections in the membranes. The linearized data is shown in Fig. 6. For Pyranine, the slope of the linearization is noticeably higher for the ESPA2 tests compared to FT30, and the ESPA2 data deviates from linearity at lower water fluxes. As was predicted by Eq. 16, the relation between $\ln(S_o J_v / R_o)$ and flux is logarithmic instead of linear in the presence of imperfections. The resulting permeability coefficients and external mass transfer coefficients of the linearization are shown in Table 1. The ESPA2 membrane is 2 to 3 times as permeable than the FT30 membrane, as expected. Interestingly, the ESPA2 membrane appeared to be more prone to ECP than the FT30 membrane, with lower external mass transfer coefficients of both NaCl and Pyranine at 0.4 m/s crossflow velocity. It is unlikely that this difference is purely experimental error: the tests were performed under identical conditions in a temperature-controlled system, with reproducible feed flow rates delivered by a positive displacement pump controlled using a variable frequency drive. Other possible explanations include a different membrane surface roughness or different compaction behaviour which would change the membrane surface. Since this is outside of the scope of the current study, this was not investigated in further detail.

Using the external mass transfer coefficients of NaCl and Pyranine, the proportionality with diffusivity and the exponent of the Schmidt number can be determined (see Eq. 20). The aqueous diffusivity of NaCl and Pyranine are 1.51 and $0.478 \cdot 10^{-9}$ $m^2/s$ respectively. This yielded exponents of 0.375 and 0.188 for FT30 and ESPA2, respectively. The Schmidt number exponent for the FT30 membrane is within the expected range: it is in between the value of 0.33 for fully developed laminar flow [29, 31] and 0.4 for turbulent flow in spacer-filled channels [19]. Thus, there is no experimental evidence of small imperfections for

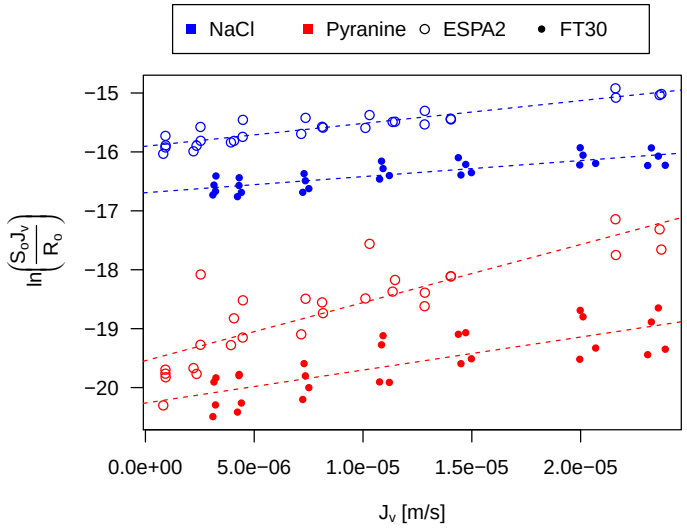


Figure 6: Linearized passage over rejection data for NaCl and Pyranine, with the fits of Eq. 14 shown as dashed lines. Note the deviation of linearity of Pyranine for the ESPA2 membrane at low flux, and the higher slope of the fit compared to the FT30 Pyranine data.

Table 1: Fitted membrane permeability coefficients and external mass transfer coefficients (at 0.4 m/s crossflow velocity, no feed spacer) .

| | $B$ (m/s) | | $k$ (m/s) | |
|---|---|---|---|---|
| Solute | ESPA2 | FT30 | ESPA2 | FT30 |
| NaCl | $1.24\pm0.05\cdot10^{-7}$ | $5.63\pm0.28\cdot10^{-8}$ | $2.58\pm0.21\cdot10^{-5}$ | $3.66\pm0.48\cdot10^{-5}$ |
| Pyranine | $3.25\pm0.43\cdot10^{-9}$ | $1.59\pm0.19\cdot10^{-9}$ | $1.01\pm0.12\cdot10^{-5}$ | $1.78\pm0.28\cdot10^{-5}$ |

this set of experiments. For the ESPA2 membrane however, the value is much lower than expected, which was shown in the preceding section to be caused by imperfections. Assuming that the correct exponent is 0.375, the lower exponent of 0.188 corresponds to $f_i = 86{\cdot}10^{-6}$. This value was found by predicting the expected $k$ for Pyranine for a perfect membrane using the above Schmidt number exponent, which then served as an input in simulating an imperfection-bearing membrane. Increasing the convective contribution then lowers the apparent $k$, reaching the value of $1.01{\cdot}10^{-5}$ for $f_i = 86{\cdot}10^{-6}$. In assuming that 0.375 is the correct Schmidt number exponent, it is taccitly assumed that the FT30 coupons are imperfection-free. This cannot be guaranteed; there is rather no experimental evidence of imperfections within the achieved experimental accuracy.
Using this value of $f_i$, the contributions of convective transport and solution-diffusion transport to the total passage of Pyranine were calculated, shown in Fig. 7. At a flux of 10 µm/s (=36 lmh), the contribution of imperfections to total passage was estimated at 21%. This shows that solutes for which the membrane displays a non-zero permeability can be used for integrity monitoring, and that the increased passage can deliver a quantitative estimate of the amount of permeate originating from convective flow through imperfections. The ESPA2 coupons showed a higher water and NaCl permeability compared to the manufacturer's specifications, 117% and 258% of the reported values respectively. It is clear that the comparatively small contribution of imperfections cannot explain this increased permeability, although it is possible that the higher-than-expected permeability correlates with the presence of imperfections. Degradation of the active layer will gradually increase permeability before forming imperfections, as shown by Antony et al. [22] who progressively degraded RO membranes using hypochlorite until almost no selectivity against NaCl remained. The membranes in this study were not intentionally damaged, but damage could have been caused during storage or by handling of the membrane coupons.

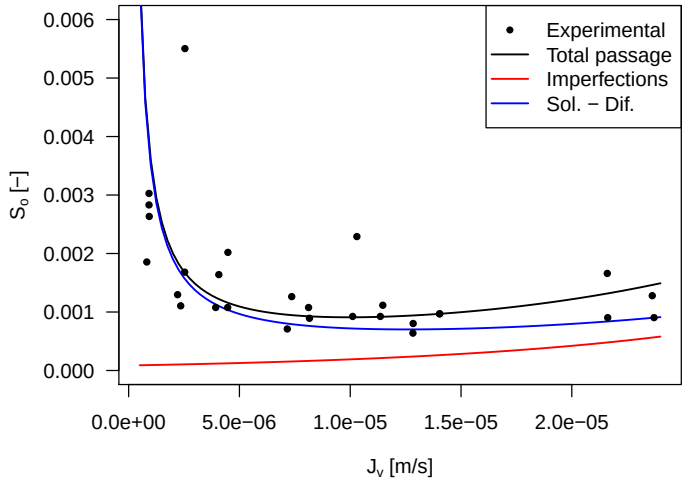


Figure 7: The contributions of convective transport and solution-diffusion transport to Pyranine passage as a function of flux for the ESPA2 experiments, based on an estimate of $f_i = 86{\cdot}10^{-6}$.

## 4.5 Error propagation in experimental data and in estimates of $f_i$

The equations used to fit $k$, $B$ and $f_i$, Eqs. 14 and 16, take as dependent variable the ratio of passage over rejection. Passage and rejection are in turn ratios of experimentally determined solute concentrations, so measurement error propagates through two consecutive divisions. To examine the effect of error propagation on $f_i$ estimates, a Monte Carlo simulation was performed. Simulated data of observable rejection was generated for $f_i$ varying between $1{\cdot}10^{-6}$ to $1{\cdot}10^{-3}$, with $k$ fixed at $1{\cdot}10^{-5}$ m/s and $B$ equaling $1{\cdot}10^{-11}$, $1{\cdot}10^{-10}$ or $1{\cdot}10^{-9}$ m/s. For each combination of $f_i$, $k$ and $B$, 100 series of experiments were simulated. Each experimental series consisted of 10 datums: observable passage as a function of flux, with the flux being random and uniformly distributed values in the interval of 1 to $10{\cdot}10^{-6}$ m/s, mimicking one series of experiments. To this simulated observable passage data, normally distributed random errors were added, with the standard deviation being either 2% or 5% of the observable passage value. Then, the same fitting procedure as described earlier was applied, i.e. fitting of $B$, $k$ and $f_i$. In Fig. 8, the mean and standard deviation of the estimated $\hat{f}_i$ is shown, normalized by the value of $f_i$ used in the Monte Carlo simulation. Fig. 8 shows that reliability of $f_i$ estimates depends strongly on the absolute value of $B$: a relatively high membrane permeability of $1{\cdot}10^{-9}$ only yields reliable $f_i$ estimates for $f_i > 5{\cdot}10^{-5}$, even for low experimental error. Experimental error up to 5% in combination with a low membrane permeability is shown here to have a negligible effect on the accuracy of $f_i$ estimates. Experimental error was assumed to be proportional to the absolute value of passage (and thus to concentration), while relative error of an analytical technique generally increases at the lower end of the concentration range of said

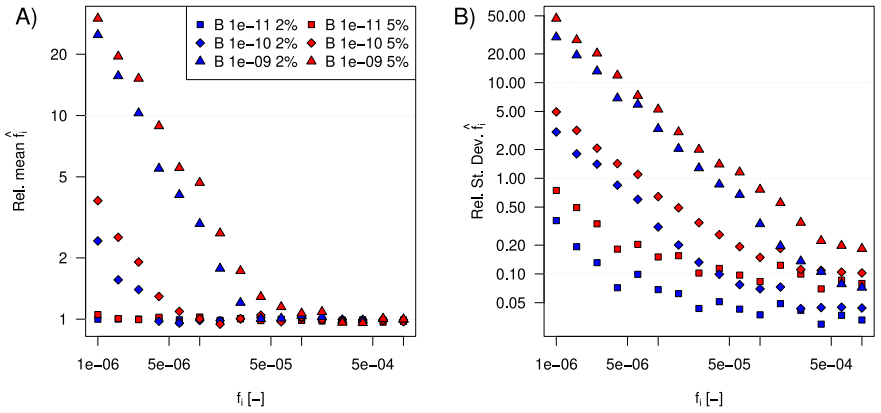


Figure 8: Relative mean (A) and relative standard deviation (B) of estimated $f_i$ for $f_i$ varying between $1{\cdot}10^{-6}$ to $1{\cdot}10^{-3}$ using Monte Carlo simulation. Normally distributed errors were introduced in the simulation data, with a relative error of 2 or 5% on the simulated solute passage.

technique. This was not included in this simulation, as such considerations are too specific, and because there are various methods of extending the range of analytical techniques through sample preparation. On the high concentration end (feed samples), samples can be diluted prior to analysis or analyzed using less sensitive techniques (e.g. light absorption instead of fluorescence), while on the low concentration end, samples can be concentrated through for instance solid phase extraction or (partial) evaporation. This allows analytical range to span many orders of magnitude, albeit at increased sample preparation effort.

## 4.6 Are certain solutes only permeating through imperfections?

Since for a given large solute neither the membrane permeability coefficient or exact external mass transfer coefficient are known a priori, and for a given membrane the presence or absence of small imperfections is unknown, we could in theory consider a membrane to be impermeable to the given solute, but containing sparse imperfections through which the solute permeates. On the other hand, we can consider a membrane imperfection-free but assign a non-zero permeability to the given solute. Can both scenarios be distinguished based on data of solute passage as a function of water flux?

In this study, we presented three phenomena related to solute passage that are distinct for imperfection-bearing membranes. These are: non-linearity of $\ln(S_o J_v / R_o)$ as a function of flux, larger solutes displaying a passage as high or higher than the passage of smaller solutes, and an unexpectedly low exponent of the Schmidt number when comparing the external mass transfer coefficient between different solutes. In the case of the passage of large solutes overtaking smaller solutes, this was not experimentally confirmed in this study, and appears only to be occurring at high contributions of imperfections to water flux. The

other 2 phenomena were observed in this study. Of these, the finding of a reduced Schmidt number exponent is deemed more robust: it does not require experimental data at very low fluxes, and by comparing the experimental data of multiple solutes, the impact of experimental error is reduced. Additionally, the range of expected Schmidt number exponents is rather narrow, and is limited on the lower end by mass transfer relations developed for laminar flow, which are well rooted in transport theory.
However, if there is no passage data available of multiple solutes, or if the diffusivity of tracers is unavailable, there is no straightforward method to discern between diffusive solute transport through intact active layer and convective transport through imperfections. In Figs. 5 and 6, the Pyranine passage data of the FT30 and ESPA2 coupons looks highly similar, and the difference between them could be easily justified by the overall higher permeability of the ESPA2 membrane. It is only when the Schmidt number exponent was quantified that proof of convective transport was found.

# 5 Conclusions

In this study, it is shown that imperfections in RO membranes can contribute significantly to solute passage if the membrane permeability is low enough. At the same time, the contribution of imperfections to the passage of smaller solutes for which the membrane is relatively permeable is negligible, showing that passage of small solutes such as NaCl cannot be used for integrity monitoring. In the range of imperfections contributing $10^{-6}$ to $10^{-3}$ to permeate flow rate, the membrane permeability of the tracer should not be higher than $10^{-9}$ m/s for accurate quantification, provided analytical techniques allow for low enough LOQs.
Discriminating between the expected permeability of a membrane, external concentration polarization and convective transport through imperfections is possible thanks to mass transport phenomena unique to imperfections. We have identified 3 such phenomena:

1. Non-linearity of $\ln(S_o J_v / R_o)$ as a function of flux, which becomes a logarithmic relation in the presence of imperfections. The non-linearity is most noticeable when solute passage is measured at a wide range of water fluxes, and must include low water fluxes. This was experimentally observed in this study.

2. Identical passage of solutes with varying size or diffusivity, or larger solutes "overtaking" smaller solutes in passage. This was not experimentally observed, but has been reported earlier [5].

3. Remarkably low estimate of the Schmidt number exponent when comparing the external mass transfer coefficient of multiple solutes, or conversely, a high apparent proportionality between the external mass transfer coefficient and solute diffusivity. This was observed, and is also deemed the most reliable method of quantifying the contribution of imperfections to water flux. This method can be applied on large datasets consisting of multiple solutes with passage measured at multiple fluxes, thereby increasing the reliability of quantifying imperfections.

There is no a priori knowledge of the membrane permeability coefficient or external mass transfer coefficient needed, only the solutes' diffusivity must be known. Therefore, the methods outlined in this paper are broadly applicable to fluorescence membrane integrity monitoring, and can be applied in real-time.

# 6 Acknowledgments

ADH wants to acknowledge FWO project G0D5119N "Bringing FO to market". AY wants to acknowledge "Resources recycling from agri-food, urban and industrial wastes by integration of hybrid separation processes (Waste for Value, W4V) (project PID2020-114401RB-C21 funded by the Spanish Research Agency (AEI) and by the Catalan Government through the SRG program (2017-SGR-312)

# 7 References

## References


[1] M.-L. Pype, B. C. Donose, L. Martí, D. Patureau, N. Wery, W. Gernjak, Virus removal and integrity in aged RO membranes, Water Research 90 (2016) 167–175. doi:10.1016/j.watres.2015.12.023.

[2] R. S. Trussell, R. A. Tackaert, A. N. Pisarenko, E. Y. Idica, R. R. Trussell, J. Minton, Realizing Reverse Osmosis Potential for Potable Reuse: Demonstrating Enhanced Pathogen Removal, Tech. Rep. DWPR 196, Bureau of Reclamation, U.S. Department of the Interior, Denver, USA (2017).

[3] L. M. Hornstra, T. Rodrigues da Silva, B. Blankert, L. Heijnen, E. Beerendonk, E. R. Cornelissen, G. Medema, Monitoring the integrity of reverse osmosis membranes using novel indigenous freshwater viruses and bacteriophages, Environmental Science: Water Research & Technology 5 (9) (2019) 1535–1544. doi:10.1039/C9EW00318E.

[4] M.-L. Pype, M. G. Lawrence, J. Keller, W. Gernjak, Reverse osmosis integrity monitoring in water reuse: The challenge to verify virus removal – A review, Water Research 98 (2016) 384–395. doi:10.1016/j.watres.2016.04.040.

[5] S.-H. Yoon, Potential and limitation of fluorescence-based membrane integrity monitoring (FMIM) for reverse osmosis membranes, Water Research 154 (2019) 287–297. doi:10.1016/j.watres.2019.02.001.

[6] V. S. Frenkel, Y. Cohen, New techniques for real-time monitoring of reverse osmosis membrane integrity for virus removal, Water Practice and Technology 13 (4) (2018) 947–957. doi:10.2166/wpt.2018.121.

[7] J. Zhang, M. Cran, K. Northcott, M. Packer, M. Duke, N. Milne, P. Scales, A. Knight, S. R. Gray, Assessment of pressure decay test for RO protozoa removal validation in remote operations, Desalination 386 (2016) 19–24. doi:10.1016/j.desal.2016.02.031.

[8] E. Ostarcevic, J. Jacangelo, S. Gray, M. Cran, Current and Emerging Techniques for High-Pressure Membrane Integrity Testing, Membranes 8 (3) (2018) 60. doi:10.3390/membranes8030060.

[9] M.-L. Pype, D. Patureau, N. Wery, Y. Poussade, W. Gernjak, Monitoring reverse osmosis performance: Conductivity versus fluorescence excitation–emission matrix (EEM), Journal of Membrane Science 428 (2013) 205–211. doi:10.1016/j.memsci.2012.10.027.

[10] S. Surawanvijit, J. Thompson, A. Rahardianto, V. Frenkel, Y. Cohen, Pulsed marker method for real-time detection of reverse osmosis membrane integrity loss, Desalination 370 (2015) 25–32. doi:10.1016/j.desal.2015.05.003.

[11] J. Wijmans, R. Baker, The solution-diffusion model: A review, Journal of Membrane Science 107 (1-2) (1995) 1–21. doi:10.1016/0376-7388(95)00102-I.

[12] D. Paul, Reformulation of the solution-diffusion theory of reverse osmosis, Journal of Membrane Science 241 (2) (2004) 371–386. doi:10.1016/j.memsci.2004.05.026.

[13] E. Dražević, K. Košutić, V. Kolev, V. Freger, Does Hindered Transport Theory Apply to Desalination Membranes?, Environmental Science & Technology 48 (19) (2014) 11471–11478. doi:10.1021/es502085p.

[14] R. Krishna, Describing mixture permeation across polymeric membranes by a combination of Maxwell-Stefan and Flory-Huggins models, Polymer 103 (2016) 124–131. doi:10.1016/j.polymer.2016.09.051.

[15] D. S. Dlamini, S. Levchenko, M. Bass, B. B. Mamba, E. M. Hoek, J. M. Thwala, V. Freger, Solute hindrance in non-porous membranes: An ATR-FTIR study, Desalination 368 (2015) 60–68. doi:10.1016/j.desal.2015.03.009.

[16] G. M. Geise, D. R. Paul, B. D. Freeman, Fundamental water and salt transport properties of polymeric materials, Progress in Polymer Science 39 (1) (2014) 1–42. doi:10.1016/j.progpolymsci.2013.07.001.

[17] G. Schock, A. Miquel, Mass transfer and pressure loss in spiral wound modules, Desalination 64 (1987) 339–352. doi:10.1016/0011-9164(87)90107-X.

[18] M. Mulder, Basic Principles of Membrane Technology, 2nd Edition, Kluwer Academic, Dordrecht ; Boston, 1996.

[19] C. Koutsou, S. Yiantsios, A. Karabelas, A numerical and experimental study of mass transfer in spacer-filled channels: Effects of spacer geometrical characteristics and Schmidt number, Journal of Membrane Science 326 (1) (2009) 234–251. doi:10.1016/j.memsci.2008.10.007.

[20] I. Sutzkover, D. Hasson, R. Semiat, Simple technique for measuring the concentration polarization level in a reverse osmosis system, Desalination 131 (1-3) (2000) 117–127. doi:10.1016/S0011-9164(00)90012-2.

[21] M. Kitis, J. C. Lozier, J.-H. Kim, B. Mi, B. J. Mariñas, Microbial removal and integrity monitoring of ro and NF Membranes, Journal - American Water Works Association 95 (12) (2003) 105–119. doi:10.1002/j.1551-8833.2003.tb10515.x.

[22] A. Antony, A. Branch, G. Leslie, P. Le-Clech, Impact of membrane ageing on reverse osmosis performance – Implications on validation protocol, Journal of Membrane Science 520 (2016) 37–44. doi:10.1016/j.memsci.2016.07.036.

[23] A. E. Yaroshchuk, Solution-diffusion-imperfection model revised, Journal of Membrane Science 101 (1-2) (1995) 83–87. doi:10.1016/0376-7388(94)00277-6.

[24] C. Niewersch, C. Rieth, L. Hailemariam, G. G. Oriol, J. Warczok, Reverse osmosis membrane element integrity evaluation using imperfection model, Desalination 476 (2020) 114175. doi:10.1016/j.desal.2019.114175.

[25] S. Loeb, Effect of porous support fabric on osmosis through a Loeb-Sourirajan type asymmetric membrane, Journal of Membrane Science 129 (2) (1997) 243–249. doi:10.1016/S0376-7388(96)00354-7.

[26] Y. Avnir, Y. Barenholz, pH determination by pyranine: Medium-related artifacts and their correction, Analytical Biochemistry 347 (1) (2005) 34–41. doi:10.1016/j.ab.2005.09.026.

[27] R. C. Hardy, R. L. Cottington, Viscosity of deuterium oxide and water in the range 5 to 125 C, Journal of Research of the National Bureau of Standards 42 (6) (1949) 573. doi:10.6028/jres.042.049.

[28] D. M. Malone, J. L. Anderson, Diffusional boundary-layer resistance for membranes with low porosity, AIChE Journal 23 (2) (1977) 177–184. doi:10.1002/aic.690230206.

[29] S. De, P. Bhattacharya, Prediction of mass-transfer coefficient with suction in the applications of reverse osmosis and ultrafiltration, Journal of Membrane Science 128 (2) (1997) 119–131. doi:10.1016/S0376-7388(96)00313-4.

[30] E. Lyster, Y. Cohen, Numerical study of concentration polarization in a rectangular reverse osmosis membrane channel: Permeate flux variation and hydrodynamic end effects, Journal of Membrane Science 303 (1-2) (2007) 140–153. doi:10.1016/j.memsci.2007.07.003.

[31] J. Villaluenga, Y. Cohen, Numerical model of non-isothermal pervaporation in a rectangular channel, Journal of Membrane Science 260 (1-2) (2005) 119–130. doi:10.1016/j.memsci.2005.03.025.